



Cite this: *RSC Adv.*, 2022, 12, 29677

Fabrication and characterization of novel macroporous hydrogels based on the polymerizable surfactant AAc-Span80 and their enhanced drug-delivery capacity

Kai Tu, Junyan Wu and Weixia Zhu *

In this study, macroporous pH-sensitive poly[*N*-isopropylacrylamide-co-acrylic acid-sorbitan monooleate] hydrogels, termed as PNIPAM-co-AAc-Span80 hydrogels, with an enhanced hydrophobic property and a rich pore structure were prepared by free-radical polymerization in an ethanol/water mixture. The polymerizable surfactant AAc-Span80 was obtained by the esterification of acrylic acid (AAc) and sorbitan monooleate (Span80), which was used to copolymerize with *N*-isopropylacrylamide (NIPAM). The chemical structure, thermal stability, morphology, and amphipathy of the PNIPAM-co-AAc-Span80 hydrogels were characterized. The results showed that the polymerizable surfactant AAc-Span80 macromolecule introduced into the hydrogels could not only increase the hydrophobic property but also ameliorate the porous network morphology, which was conducive to high adsorption capacity for adriamycin hydrochloride (DOX). The adsorption results showed that the equilibrium adsorption capacity of DOX reached 467.5 mg g⁻¹ within 48 h at pH 7.4, and the hydrophobic interactions and intermolecular hydrogen bonds were the main force in the adsorption process of DOX. The release results demonstrated that the macroporous pH-sensitive hydrogels loaded with DOX could release 98.7% of DOX at pH 5.0, which would be highly beneficial for the release of anti-cancer drugs in the environment of cancer cells. All the results demonstrate that the PNIPAM-co-AAc-Span80 hydrogels have great potential for the delivery of anti-cancer drugs.

Received 16th April 2022
Accepted 3rd October 2022

DOI: 10.1039/d2ra02443h

rsc.li/rsc-advances

1 Introduction

Environmentally sensitive hydrogels, also known as smart hydrogels, can undergo rapid and reversible volume changes in response to stimuli, such as temperature, pH, electrons/magnetic fields, and solvents.¹ Due to this unique property, they have been applied in many fields, such as medicine, biology, chemistry, and materials science.^{2–5} Poly *N*-isopropylacrylamide (PNIPAM) hydrogels are a widely studied type of smart hydrogel because of their temperature sensitivity, and its critical solution temperature (LCST) is around 32 °C.^{6,7} The PNIPAM gels swell and shrink across this temperature.⁸ Because of their excellent hydrophilicity, biocompatibility, and environmental sensitivity, PNIPAM hydrogels have attracted much scientific interest for domain applications in wound dressing, drug delivery, cell culture, tissue engineering, enzyme immobilization, *etc.*^{9–13} However, the response of PNIPAM hydrogels is very slow, mainly due to the formation of an impermeable surface structure that slows the outward flow of water throughout the hydrogels wrinkling phenomenon.¹⁴ On the one

hand, the response speed can be improved by surface modification, such as grafting using gold,¹⁵ silica,¹⁶ cellulose,¹⁷ or polyacetal lactone (PCL).¹⁸ On the other hand, macroporous materials can offer a mass-transfer channel and reduce the mass-transfer resistance, and thus have been widely used in medical bionics, catalysis, sensors, battery material, ion adsorptions *etc.*^{19–24} Our previous research showed that the Cr(VI) adsorption rate of macroporous hydrogels is much better than that of traditional gels.²⁵ In addition, PNIPAM hydrogels are not favorable for the transportation of hydrophobic substances because of their hydrophily. These disadvantages largely restrict the application of these hydrogels in hydrophobic separation.

Sorbitan monooleate (Span80) is a lipophilic emulsifier widely used in the pharmaceutical industry for its low concentration of nonionic surfactants.²⁶ Span80 contains abundant oxyhydroxyls and can be esterified with carboxyl groups to form a hydrophobic compound.^{27,28} In addition, some researchers proved that emulsifiers could impel the formation of a porous structure when the hydrogels polymerize.^{29,30} Inspired by this, the hydrophobic composite of Span80 was introduced into PNIPAM hydrogels to effectively increase the lipophilicity of gels and improve the mass-transfer efficiency between oil and water.

School of Chemical Engineering, Zhengzhou University, Zhengzhou 450001, Henan, China. E-mail: zhuweixia@zzu.edu.cn



In this study, we prepared a novel macroporous pH-sensitive hydrogel *via* a free-radical polymerization using NIPAM and AAc-Span80 as monomers. The polymerizable surfactant AAc-Span80 was obtained by esterifying Span80 and acrylic acid. The novel hydrogel was expected to possess better lipophilicity and porosity. To highlight the novel hydrogel (PNIPAM-*co*-AAc-Span80), the traditional ones (PNIPAM and PNIPAM-AAc) were also prepared in this study. The PNIPAM-*co*-AAc-Span80 hydrogel was characterized by Fourier transform infrared spectroscopy (FT-IR), thermogravimetric analysis (TG), and scanning electron microscopy (SEM). The swelling properties of all the gels in water solution and phemethylol solution were tested to analyze the hydrophilic and hydrophobic properties. Batch adsorption-desorption experiments of DOX in aqueous solution were performed to evaluate the drug delivery of the PNIPAM-*co*-AAc-Span80 hydrogel.

2 Experimental

2.1 Materials

N-Isopropyl acrylamide (NIPAM, 99%) was purchased from Zhengzhou Alpha Chemical Co., Ltd. Azobisisobutyronitrile (AIBN, 99.9%) was provided by Tianjin Guangfu Chemical Research Institute. Acrylic acid (AAc, AR), *N,N'*-methylenebisacrylamide (MBA, 99%), Span80 (pharmaceutical grade), and adriamycin hydrochloride (DOX) were obtained from Shanghai Aladdin Biochemical Technology Co., Ltd. Phosphate buffered saline (PBS) was purchased from Zhengzhou Alpha Chemical Co., Ltd. Toluene, ethanol, sodium carbonate, hydroquinone, and *p*-toluenesulfonic acid were all analytically pure and purchased from Tianjin Komi Chemical Reagent Co., Ltd. Water was deionized before use.

2.2 Synthesis of the polymerizable surfactant AAc-Span80

First, 4.83 g of Span80 was weighed into a 50 ml three-necked flask, and then 20 ml of toluene was added. The mixture was heated to 110 °C with stirring. Meanwhile, 0.72 g of acrylic acid, 0.04 g of hydroquinone, and 0.39 g of *p*-toluenesulfonic acid were added to the mixture. The reaction was finished when water was no longer discharged. To remove excess acrylic acid and *p*-toluenesulfonic acid, the reaction product was washed three times with sodium carbonate solution in a separatory funnel. Then, the oil phase was washed with NaCl solution to neutral. The resulting brown oil was rotary evaporated to remove the toluene, and the purified esterified product AAc-Span80 was thus obtained.

2.3 Synthesis of PNIPAM-*co*-AAc-Span80 hydrogels

Here, 0.00/0.03/0.05/0.08/0.10 g of AAc-Span80 was mixed with 10 ml of 50% ethanol solution in a 50 ml three-necked flask, and then 1.00 g of monomeric *N*-isopropylacrylamide (NIPAM), 0.02 g of the initiator azobisisobutyronitrile (AIBN), and 0.20 g of the coupling agent *N,N'*-methylenebisacrylamide (MBA) were added, respectively. The reaction was carried out at 75 °C for 3 h. After that, the products were washed with ethanol and water several times, and macroporous temperature-sensitive

amphiphilic gels of PNIPAM-*co*-AAc-Span80 were obtained. The obtained hydrogels were recorded as 00PNAS, 03PNAS, 05PNAS, 08PNAS, and 10PNAS, respectively.

2.4 Characterization

2.4.1 Swelling rate. To analyze the hydrophilic and hydrophobic properties, swelling property tests of the gels in the water solution and phemethylol solution were carried out. During the process, the dry hydrogels after lyophilization became swollen in deionized water/phemethylol for 24 h to obtain the wet weight (W_{se}).

The degree of swelling was calculated according to the following formula eqn (1):

$$\text{Swelling degree (SW)} = (W_{se} - W_0)/W_0 \quad (1)$$

where W_0 is the weight of dry hydrogels and W_{se} is the weight of swollen hydrogels at swelling equilibrium.

2.4.2 Fourier infrared spectroscopy. The chemical structures of the AAc-Span80 and PNIPAM-*co*-AAc-Span80 hydrogels were characterized by Fourier infrared spectroscopy (FT-IR, 81 M, Beijing Zhongxi Yuanda Co., Ltd.). The transmission mode was selected and scanned in the range of 400–4000 cm^{-1} .

2.4.3 Thermogravimetric analysis. Approximately 10 mg of dried the PNIPAM and PNIPAM-*co*-AAc-Span80 hydrogels were used for the thermogravimetric analysis (TGA), which was performed on a TA instrument (TMA7100, Hitachi Instruments), at a heating rate of 10 °C min^{-1} and temperature range of 30–800 °C.

2.4.4 Scanning electron microscopy. The freeze-dried PNIPAM and PNIPAM-*co*-AAc-Span80 hydrogels were carefully spread on the sample board, and then the hydrogel structure was observed by scanning electron microscopy (SEM; EVO MA15, Beijing Opal Optics Co., Ltd.).

2.4.5 Brunauer-Emmett-Teller (BET) surface area. The BET surface area of the freeze-dried hydrogels was tested using an automatic surface area analyzer (Micromeritics ASAP 2460, USA).

2.4.6 Rheological behavior. The rheological properties of the PNIPAM and PNIPAM-*co*-AAc-Span80 hydrogels were tested at 30 °C using a rotary rheometer (Anton Paar MCR 302, Austria). The frequency was 1 rad s^{-1} , and the strain scanning range was 0.1–1000%.

2.5 Adsorption experiments

2.5.1 Effect of pH. To investigate the effect of the initial pH of the adsorption solution on the adsorption amount, 0.02 g of 03PNAS was mixed with 20 ml DOX solution (0.5 mg ml^{-1}) adjusted by different pH (3.4–7.4) PBS solutions. Then the mixtures were magnetically stirred at 45 °C for 24 h. After centrifugation, the supernatant was taken out and measured with a UV-vis spectrophotometer at 480 nm. The corresponding concentration was determined through the standard curve. The adsorption capacity was calculated as follows eqn (2):

$$Q = \frac{(C_0 - C_1)v}{M} \quad (2)$$



where Q represents the cumulative adsorption capacity, C_0 means the initial concentration of DOX solution, C_1 means the concentration of DOX solution after adsorption, and M means the weight of the adsorbents.

2.5.2 Effect of temperature. To investigate the effect of temperature on the adsorption amount, 0.02 g of 03PNAS was mixed with 20 ml DOX solution (0.5 mg ml^{-1}) adjusted by PBS solution (pH 7.4). Then the mixtures were magnetically stirred at different temperature (25°C , 35°C , 45°C , 50°C , 55°C) for 24 h, respectively. The adsorption capacity was calculated as eqn (2).

2.5.3 Adsorption kinetics. To investigate the effect of the adsorption time on the adsorption amount, 0.02 g of 03PNAS was mixed with 20 ml DOX solution (0.5 mg ml^{-1}) adjusted by PBS solution (pH 7.4). Then the mixtures were magnetically stirred at 25°C and 45°C , respectively. The supernatant was collected at regular intervals to test the adsorption capacity of the 03PNAS.

The experimental data were fitted with the pseudo-first-order eqn (3) and pseudo-second-order eqn (4).

$$Q_t = Q_e(1 - e^{-k_1 t}) \quad (3)$$

$$Q_t = \frac{k_2 Q_e^2 t}{1 + k_2 Q_e t} \quad (4)$$

where $Q_e [\text{mg g}^{-1}]$ represents the equilibrium adsorption capacity, $Q_t [\text{mg g}^{-1}]$ is the adsorption capacity of DOX at a certain time $t [\text{h}]$, and k_1 and k_2 are the pseudo-first-order and pseudo-second-order models parameters of the adsorption kinetic models, respectively.

2.5.4 Adsorption isotherms. To investigate the effect of the initial concentration on the adsorption amount, 0.02 g of 03PNAS and 08PANS were mixed with 20 ml DOX solution adjusted by PBS solution (pH 7.4), respectively. DOX solutions were prepared at concentrations from 100 to 1000 mg L^{-1} . Then the mixtures were magnetically stirred at 45°C for 48 h.

The adsorption capacity was calculated as per eqn (2), and fitted by the Langmuir model and Freundlich model, as shown in eqn (5) and (6), where $Q_m [\text{mg g}^{-1}]$ and $Q_e [\text{mg g}^{-1}]$ represent

the saturated adsorption capacity and equilibrium adsorption capacity, and $C_e [\text{mg L}^{-1}]$ means the equilibrium concentration of the DOX solutions.

$$Q_e = \frac{Q_m K_L C_e}{1 + K_L C_e} \quad (5)$$

where K_L means the Langmuir constant, and

$$Q_e = K_f C_e^{\frac{1}{n}} \quad (6)$$

where K_f and n are characteristic constants for the Freundlich model related to the adsorption capacity and adsorption intensity, respectively.

2.6 Release experiments

To investigate the cumulative release rate of DOX, 20 mg of 03PNAS loaded with DOX was added to 50 ml of PBS solution (pH 5, pH 7.4) in a flask, respectively, and then magnetically stirred at 25°C , with 5 ml solutions absorbed at intervals of 1, 1, 2, 2, 4, 4, 6, 8, 12, 18, and 22 h. Meanwhile, 5 ml of PBS solution corresponding to the same pH was added to the flask. The cumulative release rate was calculated as follows eqn (7):

$$E_r = \frac{V_e \sum_{i=1}^{n-1} C_i + V_0 C_n}{M} \times 100\% \quad (7)$$

where $E_r (\%)$ is the cumulative release rate of DOX, V_0 is the total volume of the release medium, V_e is the replacement volume of PBS solution, C_n is the drug concentration released at the time of the n replacement sampling, and M is the total amount of drug loaded on the hydrogel.

3 Results and discussion

3.1 Preparation process

The preparation process for the PNIPAM-co-AAc-Span80 hydrogels included two steps as follows and as shown in Fig. 1. In the first step, under the catalysis of *p*-toluenesulfonic acid, acrylic acid (AAc) and lipophilic emulsifier sorbitan monooleate (Span80) formed the brown oil polymeric surfactant AAc-Span80

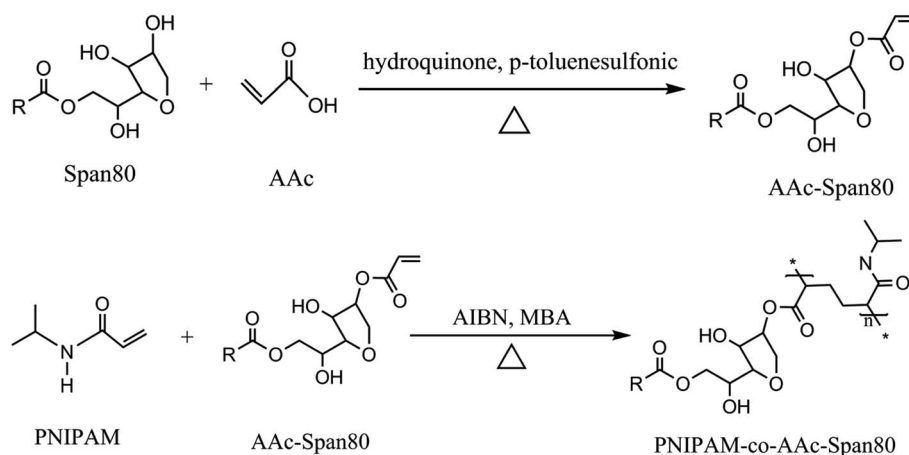


Fig. 1 Synthesis process of the PNIPAM-co-AAc-Span80 hydrogels.



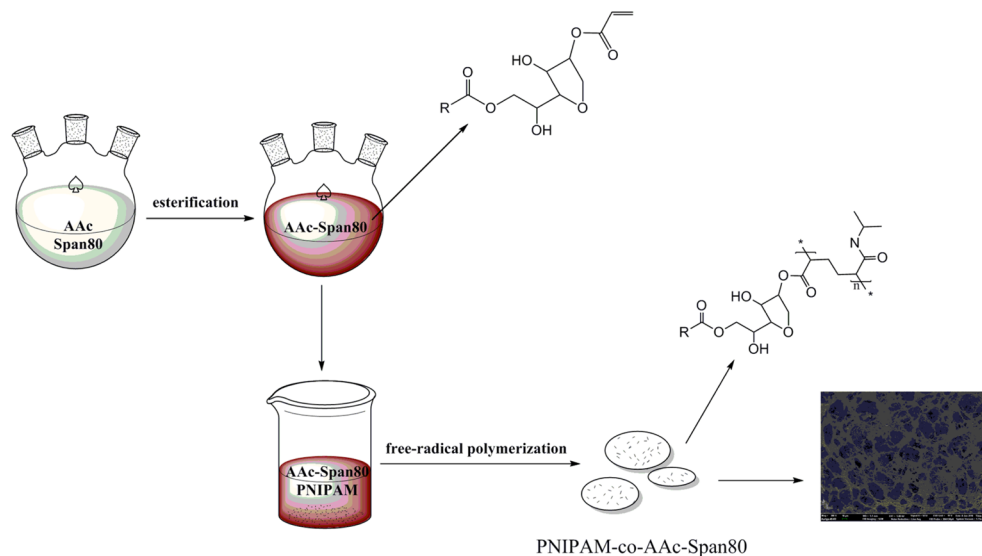


Fig. 2 Schematic illustration of the synthesis of the PNIPAM-co-AAc-Span80 hydrogels.

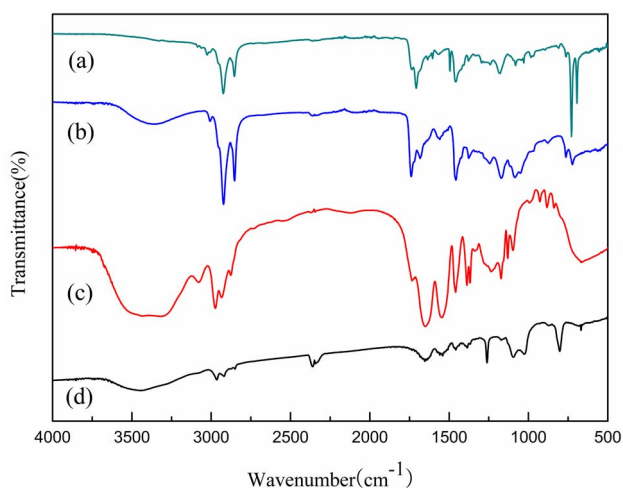


Fig. 3 FT-IR spectra of (a) Span80, (b) AAc-Span80, (c) PNIPAM-co-AAc-Span80, and (d) PNIPAM.

by esterification. In the second step, *N,N'*-methylenebisacrylamide (MBA) was chosen as a coupling agent to link the polymeric surfactant AAc-Span80 and *N*-isopropylacrylamide (NIPAM), and the PNIPAM-co-AAc-Span80 hydrogels were formed by free-radical polymerization. During polymerization, the polymeric surfactant AAc-Span80 was not only used as the hydrophobic unit but also as a micelle template to increase the porosity of the gel surface. A schematic illustration of the preparation of the PNIPAM-co-AAc-Span80 hydrogels is shown in Fig. 2.

3.2 FT-IR analysis

To verify the composition and interaction of the substances, the FT-IR spectra of (a) Span80, (b) AAc-Span80, (c) PNIPAM-co-AAc-Span80, and (d) PNIPAM hydrogels were obtained (Fig. 3). In Fig. 3(a) and (b), the stretching vibrations at 1635 and 1735

cm⁻¹ indicated the production of C=C and -O-CO in AAc-Span80. Compared with Span80, the stretching peak at 3359 cm⁻¹ related to the stretching vibration of O-H disappeared for AAc-Span80, indicating that the hydrogen bonding effect in AAc-Span80 was weakened. These results indicated that the esterification reaction of AAc and Span80 produced the hydrophobic monomer AAc-Span80. Fig. 3(c) and (d) show that PNIPAM-co-AAc-Span80 underwent stretching vibrations at 1650 and 1540 cm⁻¹, which are typical amide peaks. The stretching vibrations at 1735 and 3448 cm⁻¹ also confirmed the presence of -O-CO and O-H in PNIPAM-co-AAc-Span80, indicating that AAc-Span80 was successfully introduced into the gel network structure.

3.3 TG and DTG analysis

The TG and DTG curves for PNIPAM and PNIPAM-co-AAc-Span80 hydrogels were very similar, as can be seen in Fig. 4, demonstrating that the introduction of AAc-Span80 did not reduce the stability of the pure PNIPAM hydrogel.

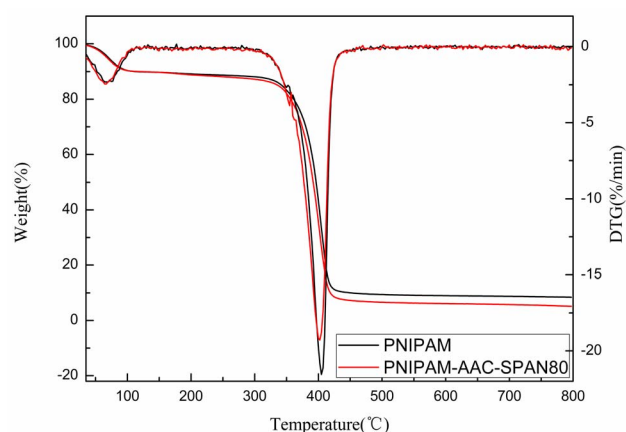


Fig. 4 TG and DTG curves of the PNIPAM and PNIPAM-co-AAc-Span80 hydrogels.



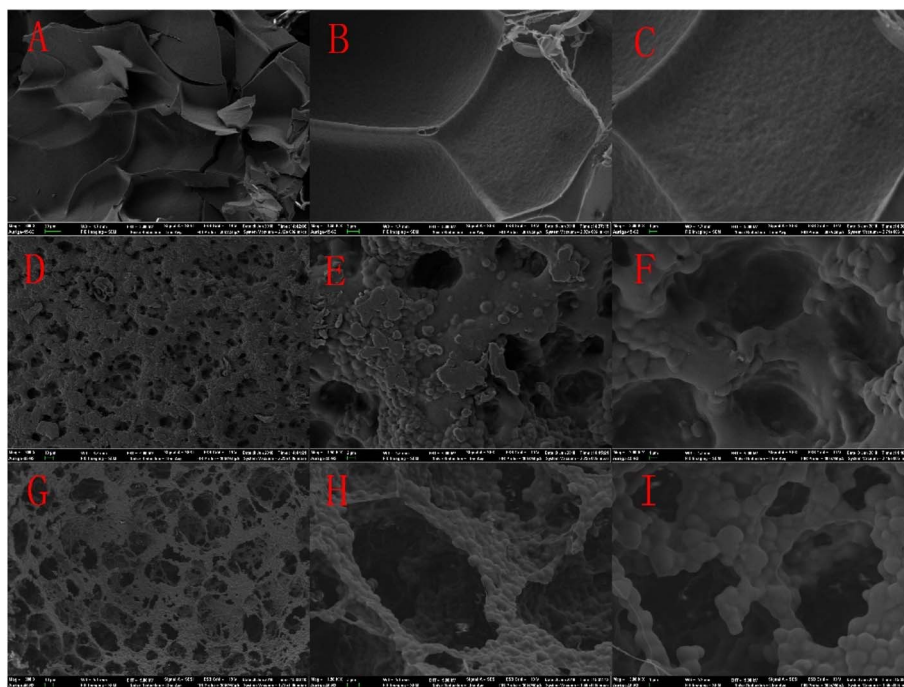


Fig. 5 SEM images of the different hydrogels: (A) 00PNAS $\times 300$, (B) 00PNAS $\times 1500$, (C) 00PNAS $\times 3000$, (D) 05PNAS $\times 300$, (E) 05PNAS $\times 1500$, (F) 05PNAS $\times 3000$, (G) 08PNAS $\times 300$, (H) 08PNAS $\times 1500$, and (I) 08PNAS $\times 3000$.

The TG and DTG curves were flat and smooth below 330 °C, and there were only two exothermic peaks in the DTG curves. These results showed that both hydrogels had good thermal stability and no impurities, and the decomposition temperature was about 350–420 °C. Generally, the pyrolysis process of the hydrogels was divided into two stages, as shown in Fig. 4: (1) the loss of moisture absorbed by the hydrogels in the temperature range 30–134 °C; (2) the degradation and carbonization of PNIPAM and PNIPAM-*co*-AAc-Span80 polymers in the temperature range 332–427 °C. These results correspond to the two peaks in the DTG curve, similar to the results reported by other researchers.^{31–34}

3.4 SEM analysis

All the samples were lyophilized to avoid changes in the network structure and pore shape. Fig. 5(A–I) show the different morphologies of the PNIPAM and PNIPAM-*co*-AAc-Span80 hydrogels. In Fig. 5(A–C), it can be seen that the surface morphology of the conventional PNIPAM gels was dense and smooth, and there were some folds but no pores. In comparison, the PNIPAM-*co*-AAc-Span80 hydrogels [Fig. 5(D–I)] possessed abundant pores and the topographies of these gels were rugged and rough. In Fig. 5(D–F), the pore size of the 05PNAS was approximately 0–20 μm with a thick pore wall. Compared to 05PNAS, the pore diameter of 08PNAS dramatically increased to 50 μm , and the pore walls were much thinner. It can be concluded that the pore volume and the number of pores gradually increased, as the amount of AAc-Span80 in the reaction solution increased. The reason for this may be due to the competitive interactions between the micellization AAc-Span80 and free-radical copolymerization between PNIPAM and AAc-Span80. The larger pore size of the hydrogels

means that the mass of AAc-Span80 plays a dominant role in controlling the pore size of the PNIPAM-*co*-AAc-Span80 hydrogels. The SEM results proved that the macromolecular emulsifier AAc-Span80 could be used as an effective porogen.

3.5 Brunauer–Emmett–Teller (BET) surface area analysis

In order to further understand the surface characteristics of the hydrogels, BET analysis was performed, with the results shown in Table 1. The results showed that the BET surface areas of 00PNAS, 05PNAS, and 08PNAS were 5.04, 15.64, and 25.84 $\text{m}^2 \text{g}^{-1}$, respectively. Also, the pore sizes of 00PNAS, 05PNAS, and 08PNAS were all between 2–50 nm. Increasing the amount of AAc-Span80 was beneficial to the generation of pores. These results were consistent with the SEM analysis results. Therefore, the polymer emulsifier AAc-Span80 could be used as an effective pore-inducing agent to increase the BET surface area and pore structure of the hydrogels.

3.6 Rheological behavior analysis of the hydrogels

The change curves for the energy storage modulus G' and loss modulus G'' of the PNIPAM and PNIPAM-*co*-AAc-Span80

Table 1 Brunauer–Emmett–Teller (BET) surface area analysis results for the hydrogels

| Sample | BET surface area ($\text{m}^2 \text{g}^{-1}$) | Pore size (nm) | Pore volume ($\text{cm}^3 \text{g}^{-1}$) |
|--------|---|----------------|---|
| 00PNAS | 5.04 | 7.61 | 0.0203 |
| 05PNAS | 15.64 | 10.79 | 0.1673 |
| 08PNAS | 25.84 | 13.72 | 0.3936 |

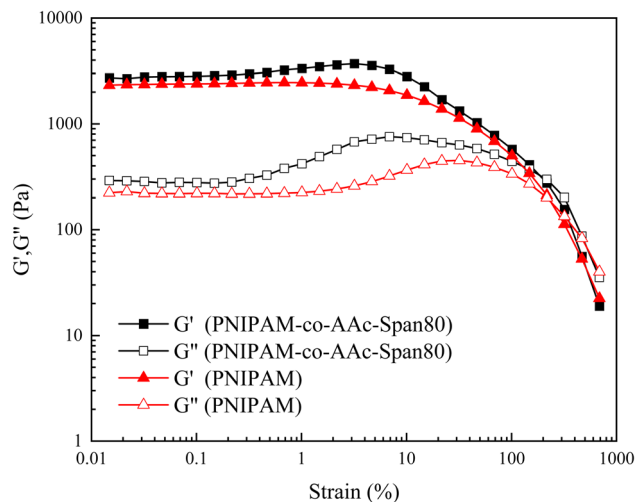


Fig. 6 Variation curves for G' and G'' of the PNIPAM and PNIPAM-co-AAC-Span80 hydrogels as a function of strain.

hydrogels with strain are shown in Fig. 6. As can be seen from Fig. 6, when the strain was small, G' was much larger than G'' , but the G' and G'' of the PNIPAM and PNIPAM-co-AAC-Span80 hydrogels were equal at about 217% strain. These results showed that the PNIPAM and PNIPAM-co-AAC-Span80 hydrogels were in a solid-like state, and the structure of the hydrogels could remain stable in this strain range. With the continuous increase in strain, the final G' was less than G'' , indicating that the structures of the PNIPAM and PNIPAM-co-AAC-Span80 hydrogels were destroyed at this point. In addition, the G' of the PNIPAM-co-AAC-Span80 hydrogels was larger than that of the PNIPAM hydrogels. This was because the introduction of AAC-Span80 increased the cross-linking degree of the copolymer as well as the pore structure, resulting in an increase in the energy storage modulus G' . Therefore, the addition of AAC-Span80 could increase the cross-linking degree of the hydrogel, and improve the structural stability of the hydrogel.

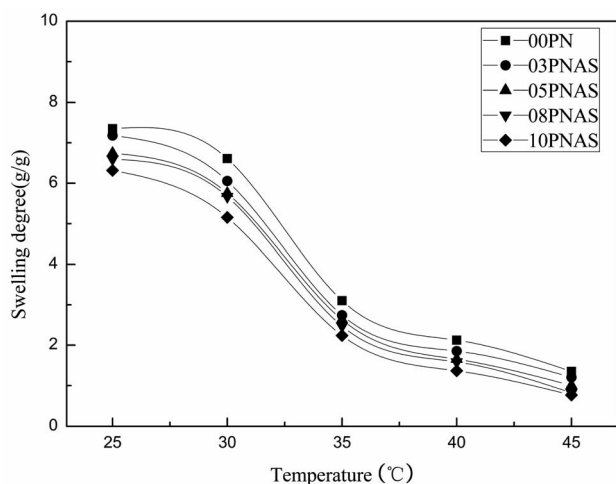


Fig. 7 Temperature sensitivity of the PNIPAM and PNIPAM-co-AAC-Span80 hydrogels in water.

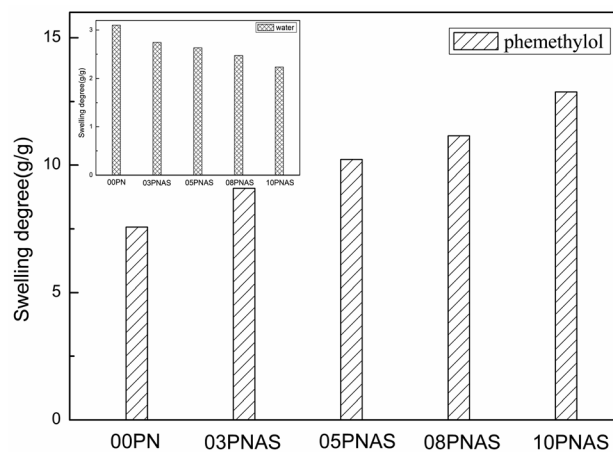


Fig. 8 Swelling degrees of the PNIPAM and PNIPAM-co-AAC-Span80 hydrogels in water/phemethylol at 35 °C.

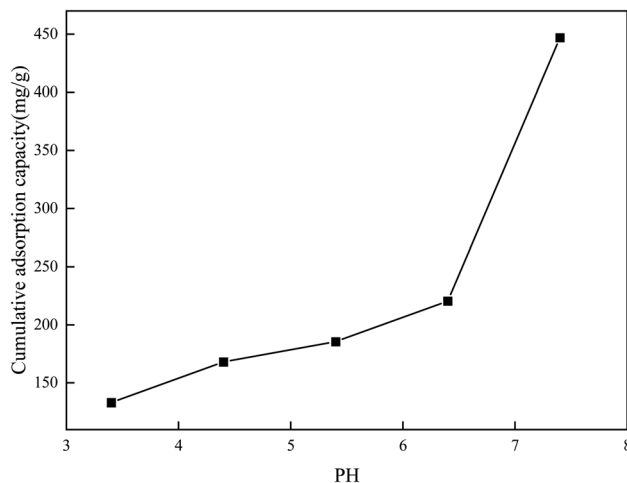


Fig. 9 Adsorption capacity of DOX on hydrogel at different pH values.

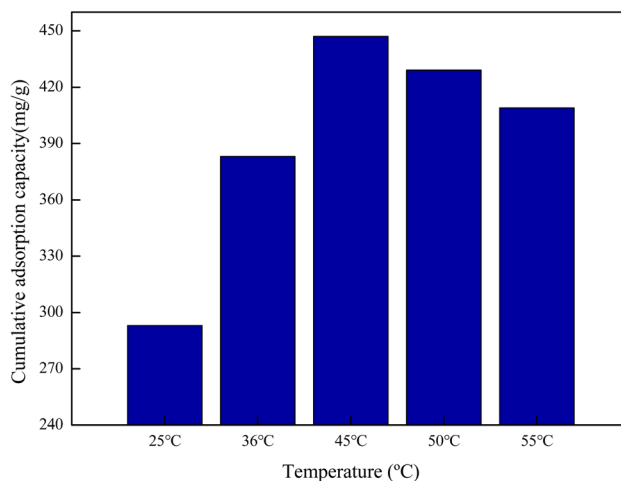


Fig. 10 Cumulative adsorption capacity of DOX on hydrogel at different temperatures.



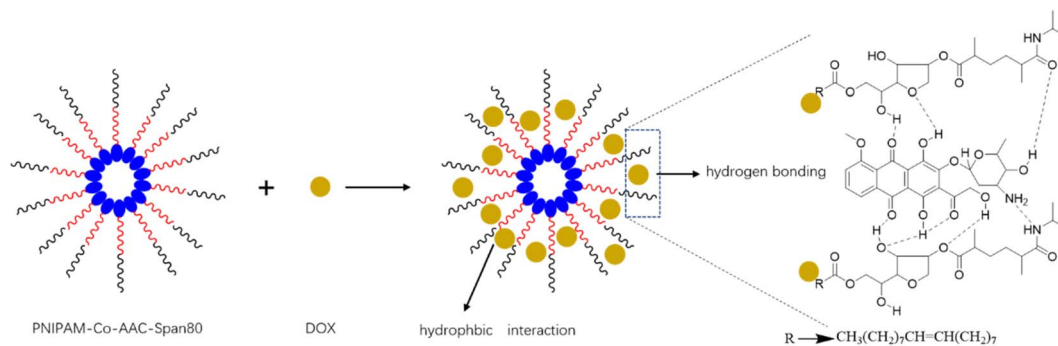


Fig. 11 DOX adsorption mechanism diagram.

3.7 Temperature sensitivity of the hydrogels

To test the temperature sensitivity of the PNIPAM-*co*-AAC-Span80 hydrogels, the swelling degree of the hydrogels in water at 25 °C, 30 °C, 35 °C, 40 °C, and 45 °C was determined. Fig. 7 shows that the swelling degree of the PNIPAM and PNIPAM-*co*-AAC-Span80 hydrogels was strongly dependent on the temperature, which gradually decreased with the temperature increasing. Among all the hydrogels, the PNIPAM hydrogels possessed the highest swelling degree in water at 25 °C over the experimental temperature range. The maximum swelling degrees of the 00PNAS, 03PNAS, 05PNAS, 08PNAS, and 10PNAS hydrogels in water were 7.34, 7.17, 6.74, 6.59, and 6.31 at 25 °C; 3.10, 2.74, 2.63, 2.47, and 2.23 at 35 °C; and 1.35, 1.20, 1.00, 0.82, and 0.76 at 45 °C, respectively. Thus, it can be concluded that the introduction of the polymeric surfactant AAC-Span80 decreased the hydrophilicity of the hydrogels, but did not change the temperature sensitivity. In addition, the swelling degree curves of the PNIPAM and PNIPAM-*co*-AAC-Span80 hydrogels were very similar and showed a sharp drop between 30–35 °C. Therefore, it can be reasonably assumed that the volume phase-transition temperature (VPTT) of the PNIPAM and PNIPAM-*co*-AAC-Span80 hydrogels is 30–35 °C. It can be concluded that the temperature sensitivity of the PNIPAM-*co*-AAC-Span80 hydrogels was similar to that of PNIPAM.

3.8 Amphiphilicity of the hydrogels

To test the changes in the hydrophilicity and lipophilicity of the PNIPAM hydrogels before and after the addition of AAC-Span80, the swelling degrees of the PNIPAM and PNIPAM-*co*-AAC-Span80 hydrogels in water/phemethylol were investigated. Fig. 8 shows the swelling degrees of the 00PNAS, 03PNAS, 05PNAS, 08PNAS, and 10PNAS hydrogels in water and phemethylol at 35 °C, respectively. It can be seen that the introduction of AAC-Span80 significantly increased the swelling degree of the PNIPAM-*co*-AAC-Span80 hydrogels in phemethylol. With the amount of AAC-Span80 increasing, the swelling degree of the PNIPAM-*co*-AAC-Span80 hydrogels in phemethylol gradually increased, and the maximum value was 12.88 for 10PNAS. In contrast, as the amount of AAC-Span80 increased, the swelling degree of the PNIPAM-*co*-AAC-Span80 hydrogels in water gradually decreased, and the minimum value was 2.23 for 10PNAS. The

amphiphilicity results proved that the polymeric surfactant AAC-Span80 could reduce the hydrophilicity of PNIPAM, and increase the lipophilicity of PNIPAM hydrogels.

3.9 Adsorption experiments for the hydrogels

3.9.1 Effect of pH on adsorption. The pH has significant effects on the performance of the amphiphilic hydrogels and the nucleophilicity of the DOX solutions. In order to explore the influence of the pH on DOX adsorption, 03PNAS was chosen as the adsorbent and the solution pH levels were adjusted by PBS solutions with different pH values. The results are shown in Fig. 9.

As we can see, with the increase in pH, the adsorption capacity increased. The adsorption capacity of DOX reached 447 mg g^{−1} when the pH value was 7.4. When the pH values were between 6.4 and 7.4, the adsorption amount dramatically changed. This may be because PNIPAM-*co*-AAC-Span80 hydrogels and DOX contain lots of hydroxyl groups (−OH), secondary amine groups (−NH−), and amine groups (−NH₂). In the pH 7.4 environment, the hydroxyl groups (−OH), secondary amine groups (−NH−), and amine groups (−NH₂) can form intermolecular hydrogen bonds, which is beneficial for the adsorption amounts. However, with the pH decreasing, free hydrogen ions

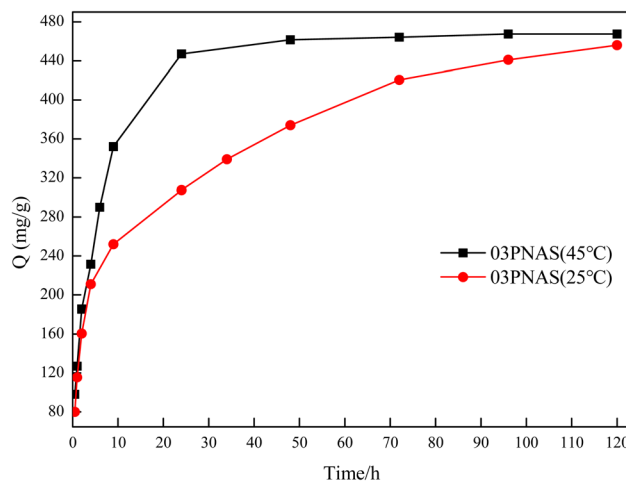


Fig. 12 Adsorption kinetics curves of DOX on hydrogels.



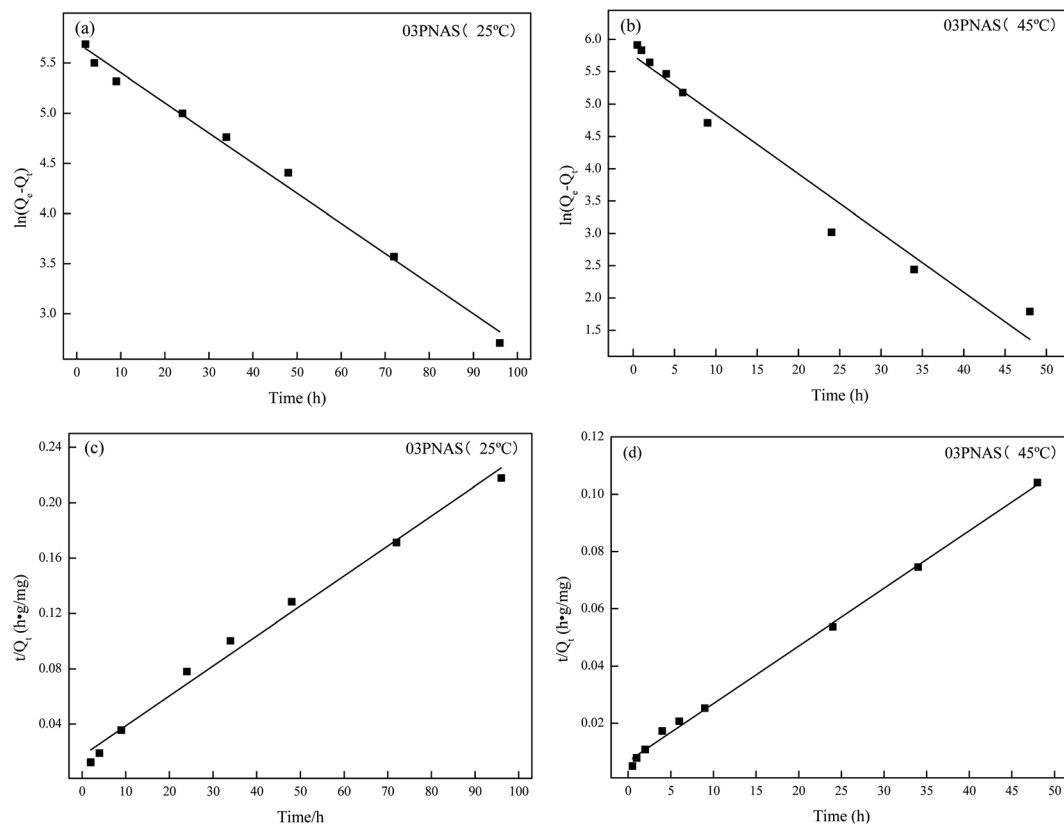


Fig. 13 Adsorption kinetics model fitting: (a) and (b) pseudo-first-order model; (c) and (d) pseudo-second-order model.

increase and cover the negative atoms on both sides, resulting in a reduction of the hydrogen bonds and hence the DOX adsorption capacity.

3.9.2 Effect of temperature on adsorption. Temperature can change the swelling degree of amphiphilic PNIPAM-*co*-AAc-Span80 hydrogels. The influence of temperature on DOX adsorption was thus explored and the results are shown in Fig. 10. It can be seen that the hydrogel eventually had an optimum DOX accumulative adsorption capacity of 447 mg g^{-1} at 45°C . This is because the molecular structure of the PNIPAM-*co*-AAc-Span80 hydrogels contained hydrophobic isopropyl and alkyl long chains, and hydrophilic amide groups and hydroxyl groups. When the temperature was low, the hydrogen bonds between the water molecules and polymer chains and the hydrogen bonds between the polymer chain coordinate with each other to form a stable hydration structure of bound water molecules around the hydrophobic groups. Meanwhile, the amide groups and hydroxyl groups present a hydrophilic state on the surface and can form a water layer on the polymer surface by hydrogen bonds with water molecules, which is unfavorable for DOX adsorption. As the temperature increased, the hydrophobic isopropyl and alkyl long chains are on the surface, and DOX could combine with the polymer through hydrophobic interaction and partial hydrogen bonding. However, excessive temperature can destroy the intermolecular hydrogen bonds between the hydrogels and DOX. That is why the accumulative adsorption capacity slightly decreased when

the temperature increased to higher than 45°C . Therefore, the hydrophobic interaction and intermolecular hydrogen bonds were the main binding force between PNIPAM-*co*-AAc-Span80 and DOX. The adsorption mechanism is shown in Fig. 11.

3.9.3 Adsorption kinetics study. The influence of the contact time on saturated adsorption is of great importance. Fig. 12 shows the effects of the DOX adsorption time on the hydrogels at different temperatures. The adsorption capacity of DOX on 03PNAS increased rapidly within 24 h and reached equilibrium at 48 h, and the final adsorption capacity reached 467.5 mg g^{-1} . Compared with at 25°C , the adsorption rate was faster in the first 24 h at 45°C . This is because the temperature increase accelerated the DOX molecules movement and increased their collisions with the gels. As for DOX adsorption at 25°C and 45°C , the adsorbents demonstrated similar behaviors. The adsorption process could be divided into two stages: first, the DOX molecules were transferred to the external

Table 2 Linear fitting parameters of the DOX adsorption kinetics of the hydrogel

| Sample | Pseudo-first-order model | | Pseudo-second-order model | |
|--------------------|--------------------------|-------|---------------------------|-------|
| | $K_1 (\text{h}^{-1})$ | R^2 | $K_2 (\text{h}^{-1})$ | R^2 |
| 25°C | 0.0301 | 0.98 | 0.0003 | 0.99 |
| 45°C | 0.0915 | 0.96 | 0.0006 | 0.99 |



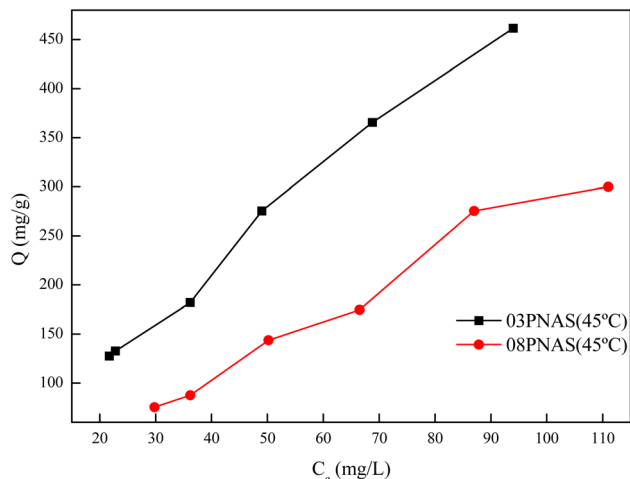


Fig. 14 Adsorption isotherms of DOX on hydrogels.

surface of the adsorbent, which is called a surface diffusion process, and then in the second stage, the DOX molecules permeated into the pores of the 03PNAS gels and diffused inside the gels, named as an internal diffusion process, which is a low diffusion process.

In order to further analyze the measured adsorption kinetics data, the pseudo-first-order kinetics model and pseudo-second-order kinetics model were used for linear fitting of the

adsorption data, as shown in Fig. 13. The calculation kinetics parameters are listed in Table 2. The adsorption data for the two models had very good fitting results. From the overall comparison of the two models, both the pseudo-second-order correlation coefficients at 25 °C and 45 °C were over 0.99, and the pseudo-second-order model was found to be superior to the pseudo-first-order one, which has been widely applied to study the adsorption of drugs in recent years.

3.9.4 Adsorption isotherms study. The DOX adsorption isotherms on the hydrogels are shown in Fig. 14. It was found that the adsorption capacity of 03PNAS was better than that of 08PNAS, up to 467.50 mg g⁻¹ when the initial concentration of DOX was 500 mg L⁻¹, whereas it was only 127.51 mg g⁻¹ at the initial concentration of 50 mg L⁻¹. These results indicated that the adsorption capability of DOX was closely related with the concentration. In order to further explore the adsorption behavior and sorption mechanism, the adsorption data were fitted with the linear Langmuir and Freundlich isothermal models. The results are shown in Fig. 15 and Table 3.

From the perspective of the correlation coefficient, the R^2 values of all four curves were greater than 0.96, showing the good fitting degree. The correlation coefficient for the Freundlich isotherm adsorption model was greater than that for the Langmuir isotherm adsorption model, indicating that the Freundlich isotherm adsorption model could better fit the experimental data. This indicated that the adsorption of DOX

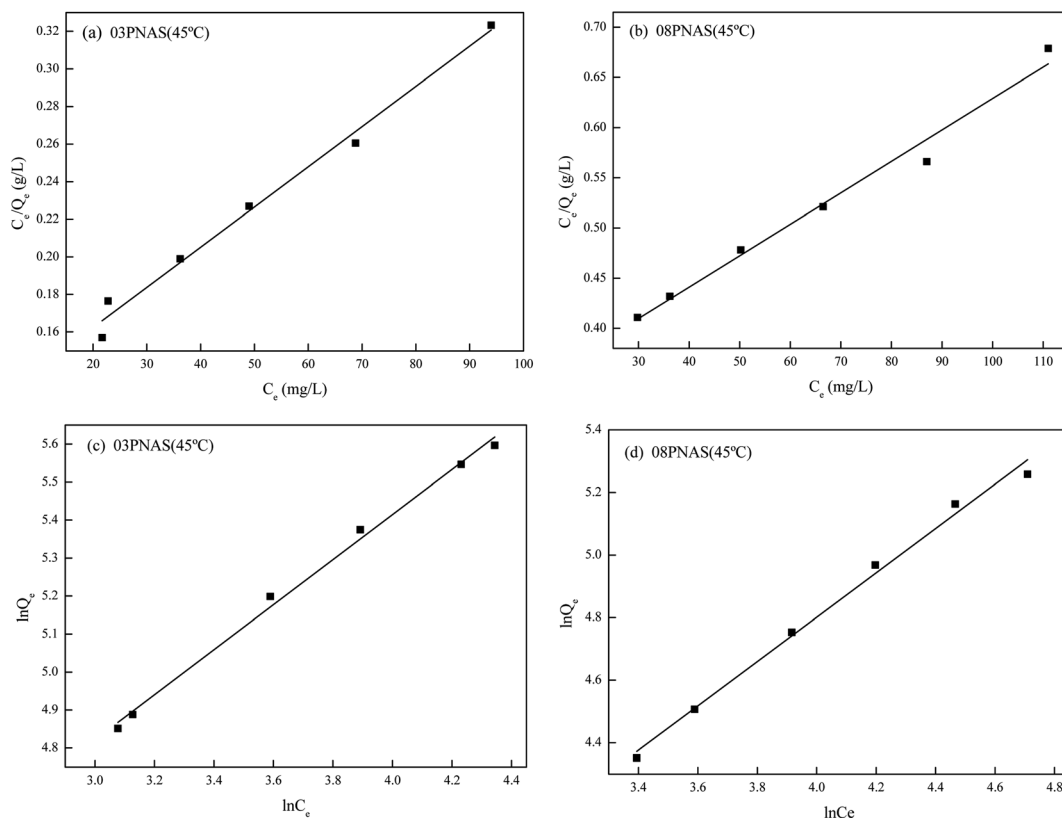


Fig. 15 Linear fitting of the DOX isothermal adsorption model by hydrogel: (a) and (b) linear fitting of the Langmuir model; (c) and (d) Freundlich model linear fitting.



Table 3 Linear fitting parameters of different models for the DOX isothermal adsorption lines of the hydrogels

| Sample | Langmuir parameters | | | Freundlich parameters | | |
|--------|----------------------------------|-----------------------------|-------|-----------------------|-------|-------|
| | Q_{\max} (mg g ⁻¹) | K_L (L mg ⁻¹) | R^2 | K_f | $1/n$ | R^2 |
| 03PNAS | 476.2 | 0.0176 | 0.98 | 20.91 | 0.59 | 0.99 |
| 08PNAS | 322.6 | 0.0099 | 0.97 | 7.142 | 0.71 | 0.99 |

onto 03PNAS and 08PNAS hydrogels strongly followed a monolayer adsorption. The adsorption between the DOX and hydrogels was diverse, and different adsorption points had different adsorption capacities. The results were consistent with the effect of temperature on the adsorption described in Section 3.9.2. In addition, the value of the Freundlich isothermal adsorption model parameter $1/n$ for 03PNAS was 0.59, indicating that the 03PNAS hydrogel had a favorable adsorption performance for DOX.

3.10 Release experiments

Release experiments can demonstrate the desorption ability of a drug, which is highly important for the evaluation of the drug-delivery effect. The curves of the cumulative release amount and time of DOX on the hydrogels are shown in Fig. 16. As can be seen from the curves, DOX was released rapidly in the first 20 h and then the release gradually slowed down. In the release environment at pH 7.4, the cumulative release of DOX in the first 20 h was 51.5%, and the final cumulative release was 66.7%. However, in the release environment of pH 5, the cumulative release of DOX in the first 20 h was 85.6%, and the final cumulative release was 98.7%. In the neutral environment, the drug diffused outward due to the concentration difference, but the complete release of the drug was prevented due to the hydrogen bond interaction between the organic shell and DOX. In the acidic environment, the hydrogen bond interaction was destroyed due to protonation of the organic shell, and the

cumulative release of DOX was significantly increased. These results are consistent with those in Section 3.9.1. These results show that 03PNAS had a pronounced pH sensitivity for DOX release, which indicated that the 03PNAS hydrogels have great potential in tumor drug delivery.

4 Conclusion

A hydrophobic composite of Span80 was successfully introduced into the PNIPAM hydrogels by esterification and free-radical polymerization, and novel amphiphilic hydrogels (PNIPAM-co-AAC-Span80) were obtained. The amphiphilicity results showed that the lipophilicity of the PNIPAM-co-AAC-Span80 hydrogels increased and their hydrophilicity decreased, because of the introduction of the hydrophobic emulsifier AAC-Span80. In addition, AAC-Span80 was used as a micelle template during polymerization, and the surface of the hydrogels became rough and porous. The pore diameter of PNIPAM-co-AAC-Span80 hydrogels was 0–50 μm when the mass ratio of NIPAM and AAC-Span80 was 1 : 0.08. The results of the DOX adsorption tests showed that the equilibrium adsorption capacity of DOX reached 467.5 mg g⁻¹ because of the formation of intermolecular hydrogen bonds between AAC-Span80 and DOX, while the DOX-release experiments indicated that 03PNAS had an obvious pH sensitivity and the cumulative release was 98.7%. In conclusion, the novel PNIPAM-co-AAC-Span80 hydrogels have great potential in anti-cancer drug delivery and expand the application of hydrogels in the biomedical field.

Author contributions

Kai Tu: methodology, writing—original draft, writing—review & editing. Junyan Wu: writing—original draft. Weixia Zhu: writing—review & editing, supervision.

Conflicts of interest

Authors declare that there is no conflict of interest.

Acknowledgements

The authors are grateful for the financial support provided by the National Natural Science Foundation of China Projects (21706240) and the convenience of SEM from analysis and testing center of Zhengzhou University.

References

- 1 P. Liu, W. Gao, Q. Zhang, K. Chen, J. Zhang, L. Chen, X. Zhang and K. Wang, *React. Funct. Polym.*, 2015, **89**, 1–8.
- 2 L. L. Wang, J. J. Chung, E. C. Li, S. Uman, P. Atluri and J. A. Burdick, *J. Controlled Release*, 2018, **285**, 152–161.
- 3 Y. Zheng, K. Huang, X. You, B. Huang, J. Wu and Z. Gu, *Int. J. Biol. Macromol.*, 2017, **104**, 1143–1149.
- 4 J. Bo, X. Luo, H. Huang, L. Li, W. Lai and X. Yu, *J. Power Sources*, 2018, **407**, 105–111.

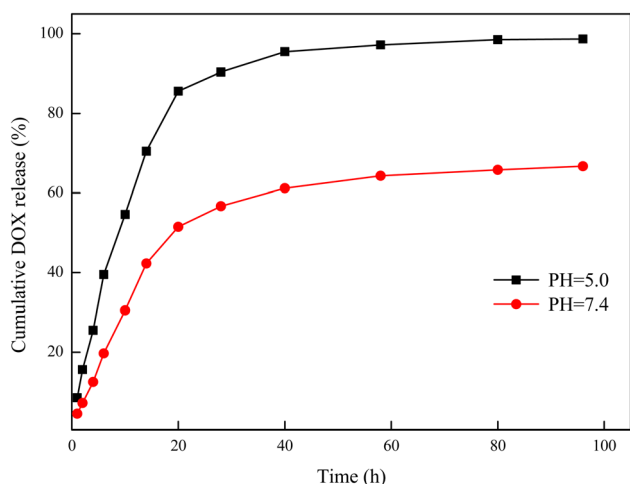


Fig. 16 DOX-release curves of drug-loaded hydrogels.



- 5 X. J. Liu, X. Y. Ren, S. Guan, H. Q. Li, Z. K. Song and G. H. Gao, *Eur. Polym. J.*, 2015, **73**, 149–161.
- 6 H. Zheng, S. Zhang, C. Yang, H. Yin, W. Liu and K. Lu, *J. Mol. Liq.*, 2021, **342**, 117551.
- 7 O. R. M. Metawea, M. A. Abdelmoneem, N. S. Haiba, H. H. Khalil, M. Teleb, A. O. Elzoghby, A. F. Khafaga, A. E. Noreldin, F. Albericio and S. N. Khattab, *Colloids Surf., B*, 2021, **202**, 111694.
- 8 H. Lai and P. Wu, *Polym*, 2010, **51**, 1404–1412.
- 9 S. L. Tomić, M. M. Mičić, S. N. Dobić, J. M. Filipović and E. H. Suljovrujić, *Radiat. Phys. Chem.*, 2010, **79**, 643–649.
- 10 A. Adibfar, G. Amoabediny, M. B. Eslaminejad, J. Mohamadi, F. Bagheri and B. Z. Doulabi, *Mater. Sci. Eng., C*, 2018, **93**, 790–799.
- 11 D. Giaouzi and S. Pispas, *Eur. Polym. J.*, 2021, **155**, 110575.
- 12 C. Cunha, P. Klein, C. Rosenauer, U. Scherf and J. S. Seixas de Melo, *Macromol*, 2021, **54**, 7612–7620.
- 13 N. Milašinović, Z. Knežević-Jugović, Ž. Jakovljević, J. Filipović and M. K. Krušić, *Chem. Eng. J.*, 2012, **181**, 614–623.
- 14 M. A. Haq, Y. Su and D. Wang, *Mater. Sci. Eng., C*, 2017, **70**, 842–855.
- 15 K. Keerati, P. Sae-ung, N. Niamnont, K. Wongravee, M. Sukwattanasinitt and V. P. Hoven, *Langmuir*, 2013, **29**, 12317–12327.
- 16 P. Zhuang, A. Dirani, K. Glinel and A. M. Jonas, *Langmuir*, 2016, **32**, 3433–3444.
- 17 L. Yang, J. Zhang, J. He, J. Zhang and Z. Gan, *Chin. J. Polym. Sci.*, 2015, **33**, 1640–1649.
- 18 J. Cao, L. Zhang, X. Jiang, C. Tian, X. Zhao, Q. Ke, X. Pan, Z. Cheng and X. Zhu, *Macromol. Rapid Commun.*, 2013, **34**, 1747–1754.
- 19 T. T. Nguyen, A. M. Rahmatika, M. Miyauchi, K. L. A. Cao and T. Ogi, *Langmuir*, 2021, **37**, 4256–4266.
- 20 Z. Zhang, G. Yi, P. Li, X. Zhang, Z. Wan, X. Wang, C. Zhang and Y. Zhang, *J. Phys. Chem. B*, 2021, **125**, 6012–6022.
- 21 Y. Dong, Z. Chen, Y. Xu, L. Yang, W. Fang and X. Yi, *Fuel Process. Technol.*, 2017, **168**, 65–73.
- 22 A. Walcarius, *TrAC, Trends Anal. Chem.*, 2012, **38**, 79–97.
- 23 F. Lapique, M. Belhadj, C. Bonnet, J. Pauchet and Y. Thomas, *J. Power Sources*, 2016, **336**, 40–53.
- 24 E. Liu, X. Xu, X. Zheng, F. Zhang, E. Liu and C. Li, *Sep. Purif. Technol.*, 2017, **189**, 288–295.
- 25 W. Zhu, H. Song, K. Du, H. Zeng and S. Yao, *J. Appl. Polym. Sci.*, 2013, **128**, 2729–2735.
- 26 K. Kato, P. Walde, N. Koine, S. Ichikawa, T. Ishikawa, R. Nagahama, T. Ishihara, T. Tsujii, M. Shudou, Y. Omokawa and T. Kuroiwa, *Langmuir*, 2008, **24**, 10762–10770.
- 27 J. F. Ontiveros, M. Nollet, C. Pierlot and V. Nardello-Rataj, *Colloids Surf., A*, 2018, **536**, 191–197.
- 28 A. M. Alsabagh, A. A. Aboulrous, M. M. Abdelhamid, T. Mahmoud, A. S. Haddad and R. Rafati, *ACS Omega*, 2021, **6**, 18668–18683.
- 29 A. Dey, R. Bera and D. Chakrabarty, *Polym*, 2017, **116**, 178–190.
- 30 S. Nishimura, T. Takami and Y. Murakami, *Colloids Surf., B*, 2017, **159**, 318–326.
- 31 K. Hemmati and M. Ghaemy, *Int. J. Biol. Macromol.*, 2016, **87**, 415–425.
- 32 K. Deshmukh, J. Ahmad and M. B. Hägg, *Ionics*, 2014, **20**, 957–967.
- 33 S. Tanpichai and K. Oksman, *Composites, Part A*, 2016, **88**, 226–233.
- 34 J. Li, C. Hu, J. Shao, H. Li, P. Li, X. Li and W. He, *Polym*, 2017, **119**, 152–159.

